Quaternary Geochronology 53 (2019) 101003

Contents lists available at ScienceDirect

Quaternary Geochronology

journal homepage: www.elsevier.com/locate/quageo

Timing and structure of the weak Asian Monsoon event about 73,000 years ago

Wenjing Du[a], Hai Cheng[a,b,*], Yao Xu[a], Xunlin Yang[c], Pingzhong Zhang[d], Lijuan Sha[a], Hanying Li[a], Xiaoyan Zhu[e], Meiliang Zhang[e], Nicolás M. Stríkis[f], Francisco W. Cruz[f], R. Lawrence Edwards[b], Haiwei Zhang[a], Youfeng Ning[a]

[a] Institute of Global Environmental Change, Xi'an Jiaotong University, Xi'an, China
[b] Department of Earth Sciences, University of Minnesota, Minneapolis, USA
[c] School of Geographical Sciences, Southwest University, Chongqing, China
[d] School of Geological Sciences and Mineral Resources, Lanzhou University, Lanzhou, China
[e] Karst Dynamics Laboratory, Institute of Karst Geology, CAGS, Guilin, China
[f] Instituto de Geociências, Universidade de São Paulo, São Paulo-SP, Brazil

ARTICLE INFO

Keywords:
Cave $\delta^{18}O$ records
GS-20 event
Structure and timing
Climate correlation

ABSTRACT

Oxygen isotope ($\delta^{18}O$) records of cave speleothem have played an important role in the past two decades in characterizing the Asian Monsoon (AM) variability and correlating the monsoonal events with other global climate events on millennial timescales. Of a series of millennial events occurred during the last glacial period, the Chinese Stadial-20 (CS-20, corresponding to the Greenland Stadial-20, GS-20) event around ~73 kyr BP (thousand years before present, where present = 1950 AD) is distinctive, since it is the weakest AM event during the last glacial period and is likely linked to the Toba volcanic super-eruption. While Greenland ice core records are commonly used to correlate the last glacial millennial events, yet their absolute age uncertainties around the GS-20 is larger than 1000 years. This prohibits precise correlations of the event between global climate archives from different climate systems to investigate the underlying climatic dynamics. Here, we present three Chinese cave stalagmite $\delta^{18}O$ records from the AM region, covering a period from 76 to 71 kyr BP, across the CS-20. All stalagmites have high uranium contents and relatively fast growth rates, allowing acquisition of high-resolution (~10 years) $\delta^{18}O$ records with precise ^{230}Th age controls (≤200 years, 2σ) to precisely characterize the structure and timing of the CS-20. Our results demonstrate that the onset and termination of the CS-20 are more gradual in Chinese cave records relative to the GS-20 event in Greenland ice core records. As such, we suggest a new 'break-point' approach to correlate CS-20 with GS-20, at either the initial onset or initial termination shifts of the events, instead of the conventional 'mid-point' match. We dated the initial onset and initial termination of CS-20 to ~74.0 ± 0.2 and 72.5 ± 0.2 kyr BP, respectively, confirming the Greenland ice core chronology well within the quoted uncertainty. The 'break-point' correlation at the GS-20/CS-20 initial termination suggests a lagged onset of CS-20 relative to the onset of GS-20. The lagged onset is in line with a northern high-latitude forcing mechanism triggering the event and a central role of oceanic reorganizations in the propagation of the climate signal. An alternative 'break-point' correlation at the GS-20/CS-20 initial onset suggests that the CS-20 initial termination leads the GS-20 initial termination by a few hundred years. This apparent paradox thus calls for further empirical and theoretical studies to better understand the underlying climatic dynamics and in turn the correlation strategy.

1. Introduction

Cave speleothem oxygen isotope ($\delta^{18}O$) records are important in delineating Asian Monsoon (AM) variations and key correlation/calibration datasets for characterizing global climate events (e.g., Wang et al., 2001, 2008; Henderson, 2006; Wolff, 2014; Cheng et al., 2006, 2009; 2012, 2016a; 2018; WAIS Divide Project Members, 2015; Buizert et al., 2015; Chen et al., 2016). This is mainly because speleothems can be dated precisely by high-precision ^{230}Th methods (e.g., Cheng et al., 2013a), and their $\delta^{18}O$ values can be rapidly analyzed for high-

* Corresponding author. No. 99 Yanxiang Road, Yanta district, Institute of Global Environmental Change, Xi'an Jiaotong University, Xi'an, 710049, China.
E-mail address: cheng021@xjtu.edu.cn (H. Cheng).

https://doi.org/10.1016/j.quageo.2019.05.002
Received 21 June 2018; Received in revised form 20 March 2019; Accepted 12 May 2019
Available online 16 May 2019
1871-1014/

resolution (e.g., Spötl and Mattey, 2006). On the other hand, the Greenland climate during the last glacial is characterized by a series of abrupt climate oscillations on millennial-scale, such as Dansgaard–Oeschger (DO) events (Dansgaard et al., 1993), or Greenland Stadial (GS) and Interstadial (GIS) events (e.g., North Greenland Ice Core Project members, 2004; Rasmussen et al., 2006, 2014; Seierstad et al., 2014). Importantly, these GS and GIS events can be correlated directly to Chinese Stadial (CS) and Interstadial events (CIS) (Cheng et al., 2006) in Chinese cave speleothem $\delta^{18}O$ records (e.g., Wang et al., 2001, 2008; Cheng et al., 2006, 2012, 2016a). In addition, many paleo-environmental archives from other climate systems can also be causally linked to Greenland ice core and Chinese cave records (e.g., Blockley et al., 2012; Cheng et al., 2012, 2016a). Such links are essential to establish a refined sequence of events and to investigate the climatic dynamics leading to occurrences of these events. Nevertheless, in order to establish such global climatic interconnections, two aspects remain critical: (1) a set of precise chronological benchmarks for correlating and calibrating climate events; and (2) an appropriate approach to link/correlate a wide range of archives obtained from different climate systems that presumably characterize different climate attributes.

Greenland ice core records are commonly used for last glacial climate correlations, because during the period these records show a number of abrupt climate events with chronologies constrained by annual layer counting. However, a critical limit is that the accumulated layer counting uncertainties increase progressively with ice core depth or time. Particularly, the reported uncertainty for the section older than 60 kyr BP (thousand years before present, where present = 1950 AD) is ~1000 years or larger (Svensson et al., 2008, 2013). The widely used Greenland ice core chronologies in the past decade are the GICC05 (e.g., Vinther et al., 2006; Rasmussen et al., 2006; Andersen et al., 2006; Svensson et al., 2008) and ss09sea model timescales (Johnsen et al., 2001; Andersen et al., 2006). The GICC05 extends just to ~60 kyr BP. The chronology of the section older than 60 kyr BP in Greenland ice cores is based on the ss09sea modelled timescale (Johnsen et al., 2001). In order to match the GICC05 at ~60 kyr BP, the older section of the ss09sea timescale was shifted by 705 years to younger side. This new chronology is denoted the GICC05modelext (Wolff et al., 2010). While the improvement of Greenland ice core chronologies continues (e.g., Rasmussen et al., 2014; Rousseau et al., 2017; Adolphi et al., 2018), up to now, the chronology of the section older than 60 kyr BP has not been considerably refined.

Additionally, how to precisely and casually correlate the abrupt changes in Greenland ice core records to the relatively gradual monsoon shifts is a critical issue to resolve. A direct correlation via absolute ages is currently unfeasible between the monsoon CS-20 and Greenland ice core GS-20 events. This is because the age uncertainties in ice core absolute chronology are considerably larger (> 1000 years) than the durations of climate shifts that we compare here. On the other hand, Chinese cave speleothem samples have great potential to date the corresponding monsoonal events (or shifts) during the last glacial with absolute errors about one magnitude smaller than those in the ice cores by using recently improved ^{230}Th dating techniques (e.g., Cheng et al., 2013a). This allows a more precise cave-based chronology beyond 60 kyr BP, which can be potentially used to calibrate the Greenland ice core chronology. Nevertheless, it remains unclear whether we can casually use the 'mid-points' to correlate relatively gradual AM shift in Chinese cave $\delta^{18}O$ records with the corresponding abrupt change of Greenland temperature in the ice core $\delta^{18}O$ records (e.g., WAIS Divide Project Members, 2015).

Of many millennial AM events in Chinese cave records in the last glacial period, a further study of the CS-20 event is important for three reasons. Firstly, the event occurred at ~73 kyr BP, when the current ice core chronological uncertainty is large due to the accumulated uncertainty from annual layer counting (e.g., GICC05modelext, Rasmussen et al., 2014; Seierstad et al., 2014). Secondly, up to now, Chinese cave records of this event have merely low $\delta^{18}O$ temporal resolutions (~40–200 years) with large dating uncertainties (~300 years or larger), and insufficient dating resolutions (1–3 dates between 74 and 72 kyr BP for each previous record) (Wang et al., 2001, 2008; Chen et al., 2016; Zhang et al., 2017). Thirdly, this event is the weakest AM event during the last glacial period in Chinese cave records (e.g., Wang et al., 2001; Xia et al., 2007; Chen et al., 2016; Zhang et al., 2017) and apparently linked to the largest volcanic eruption in the Quaternary (the Toba event) (e.g., Rampino and Self, 1992; Williams et al., 2009, 2010; Haslam and Petraglia, 2010). In this study, we report three Chinese cave $\delta^{18}O$ records from the AM region, covering a period from 76 to 71 kyr BP, across the CS-20. All of the three stalagmite sections have high uranium contents (4–20 ppm) and relatively fast growth rates, allowing high-resolution (~10 years) $\delta^{18}O$ records to be obtained with precise ^{230}Th age controls (≤200 years, 2σ). The aim of this work is to precisely characterize the structure and timing of the CS-20 event in the AM regime, test possible approaches to correlate the CS-20 with the GS-20 in the context of climate dynamics, and thus provide a chorological benchmark for correlating and calibrating climate variations surrounding the event.

2. Cave locations, samples and methods

2.1. Cave sites and stalagmite samples

Three stalagmite samples used in this study were collected from Yangkou cave (YK7 and YK02) and Wanxiang cave (WX40C), respectively. Yangkou cave (29°02′N, 107°11′E, 2140 m.a.s.l.) is in the Jinfo Mountain, Chongqing, southwestern China where the regional climate is dominated by the AM. The mean annual precipitation and temperature in the area are ~1400 mm and ~7.5 °C (Li et al., 2014). Wanxiang cave (33°19′N, 105°00′E, 1200 m.a.s.l.) is in Wudu, Gansu, central China at the summer AM fringe area where the semi-arid climate prevails (Fig. 1). The mean annual precipitation and temperature in the area are ~490 mm and ~11 °C (Zhang et al., 2008, 2010). Three stalagmites YK, YK02 and WX40C are 250, 225 and 80 mm long, respectively (Fig. S1). There are no visible hiatuses in stalagmites YK7 and WX40C (76–71 kyr BP), but a hiatus occurred at ~15 cm from top (~73 kyr BP) in stalagmite YK02.

2.2. U–Th dating

Stalagmites were first halved along growth axis and polished (Fig. S1). About 20–50 mg of powder was drilled near the central axis for each ^{230}Th dating subsample. 61 subsamples (21, 28 and 12 for stalagmites YK7, YK02 and WX40C respectively) were dated using a recently improved ^{230}Th method (Cheng et al., 2013a). Dating was performed at the Isotope Laboratory, Xi'an Jiaotong University, China. Standard chemistry procedures (Edwards et al., 1987; Cheng et al., 2000; Shen et al., 2002, 2003) were used to separate U and Th. U and Th isotopes were measured using Thermo-Scientific Neptune multicollector inductively coupled plasma mass spectrometers equipped with a MasCom multiplier behind the retarding potential quadrupole in peak-jumping mode. We followed similar procedures of characterizing the multiplier as described in Cheng et al. (2000). Instrumentation, standardization and half-lives are described in Cheng et al. (2000, 2013b). Uncertainties in U/Th isotopic data were calculated offline at 2σ level, including corrections for blanks, multiplier dark noise, abundance sensitivity, and contents of the same nuclides in spike solution. Corrected ^{230}Th ages assume the initial $^{230}Th/^{232}Th$ atomic ratio of $4.4 \pm 2.2 \times 10^{-6}$, the values for a material at secular equilibrium with the bulk earth $^{232}Th/^{238}U$ value of 3.8. Corrections are negligible due to high U and relatively low ^{232}Th contents (indicating low initial ^{230}Th) of the samples. The dating results of the three stalagmite samples are in Table S1. Age uncertainties are reported at 2σ level. All ages are in stratigraphic order within dating uncertainties. Our dating results show that all three stalagmites contain a section from 75 to 71 kyr BP across

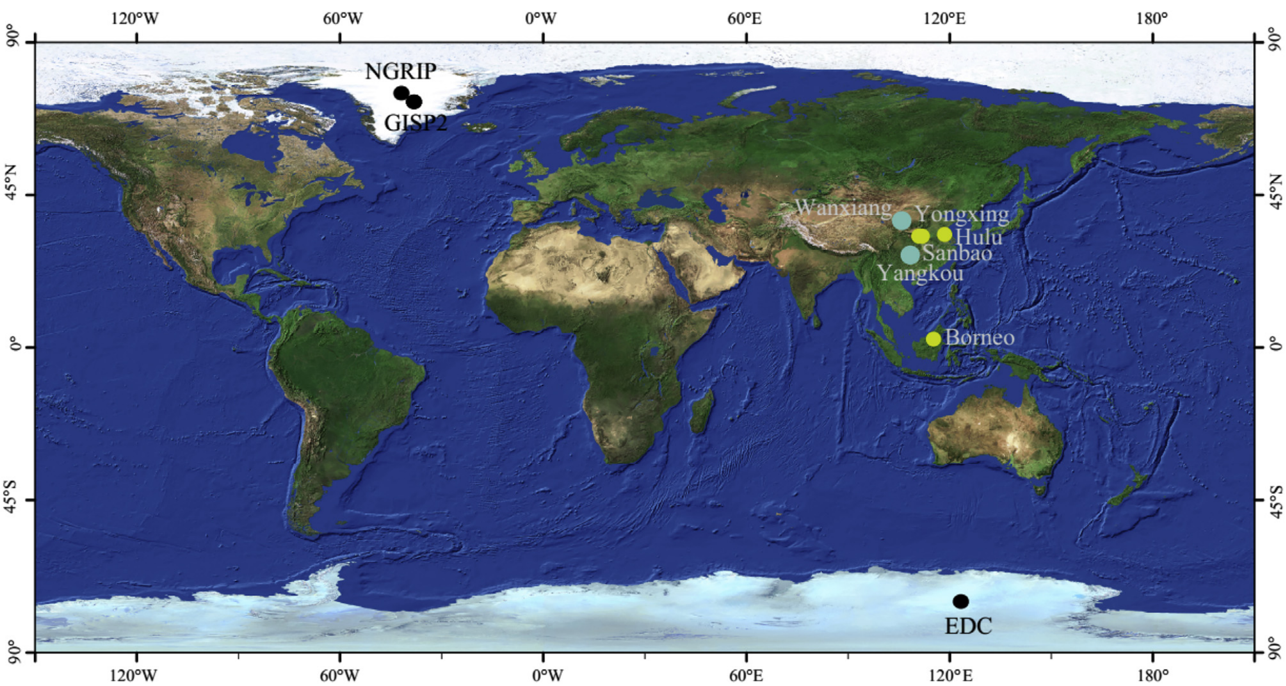

Fig. 1. Cave and ice core locations. Light blue circles indicate locations of Yangkou (29°02′N, 107°11′E) and Wangxiang (33°19′N, 105°00′E) caves (this study). Yongxing (31°35′N, 111°14′E) (Chen et al., 2016), Hulu (32°30′N, 119°10′E) (Wang et al., 2001), Sanbao (31°40′N, 110°26′E) (Wang et al., 2008) and Secret (in northern Borneo, 4°N, 115°E) (Carolin et al., 2013) caves are depicted by yellow circles. All above records cover the GS-20/CS-20 event. Black dots indicate locations of the Greenland and Antarctic ice cores in discussions.

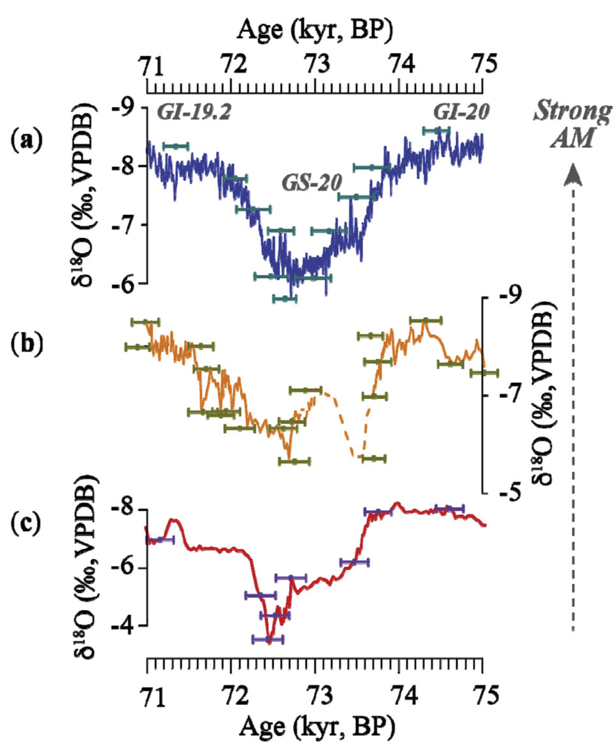

Fig. 2. Cave $\delta^{18}O$ records. (**a**)–(**c**) are YK7, YK02 and WX40C records, respectively. Error bars (2σ) show ^{230}Th dating results. The dashed curve in (**b**) indicates a slow growth section (or hiatus) in the stalagmite YK02.

the CS-20 event (Table S1 and Fig. 2).

2.3. Stable isotope analyses

The $\delta^{18}O$ values of three stalagmites were measured in three laboratories. We obtained ~2300 $\delta^{18}O$ data. About 1200 subsamples from the stalagmite YK7 were analyzed at Xi'an Jiaotong University, China using the Thermo-Scientific MAT-253 mass spectrometer connected with a Carbonate Device (Kiel-IV). The subsamples were micromilled by a New Wave Micromill along the central growth axis of the stalagmite. About 500 subsamples from stalagmite YK02 were analyzed at the University of San Paulo, Brazil using an on-line carbonate preparation system (Gasbench-II) interfaced with an isotope ratio mass spectrometer (Delta-V). The subsamples were micromilled along the extension axis of the stalagmite at ~0.2 mm increment. About 600 subsamples from the stalagmite WX40C were analyzed at Nanjing Institute of Geology and Paleontology in China, using the Thermo-Scientific MAT-253 mass spectrometer fitted with a Carbonate Device (Kiel-III). The subsamples were collected by using dental drill or graver, and the methods were described in Zhang et al. (2010). All stable isotope data are reported in per mil (‰) relative to the Vienna PeeDee Belemnite (VPDB) standard (Table S2). Standard measurements of $\delta^{18}O$ values in above three laboratories show a long-term reproducibility of ~0.1‰ or better (1σ).

2.4. 'Break-point' determination and correlation

In order to objectively assess the timings of the initial onset and termination of the GS-20/CS-20 events in Greenland ice core and our cave records (Fig. 3), we applied a statistical regression approach using the RAMPFIT (Mudelsee, 2000). This method is commonly used to determine the 'break-point' in various proxy time series (e.g., Fleitmann et al., 2003; Steffensen et al., 2008; Jiang et al., 2012). In principle, the method uses a continuous function consisting of two linear parts that are joined at the 'break-point'. The break model is fitted to data using a weighted least-squares method with a brute-force search for the 'break-point' (or the 'change-point').

We suggest to correlate $\delta^{18}O$ records from Chinese caves and Greenland ice cores via their 'break-points', instead of the commonly-used 'mid-points'. The basic concepts related to this approach are illustrated in Fig. 3. The assumption of the 'break-point' synchronies

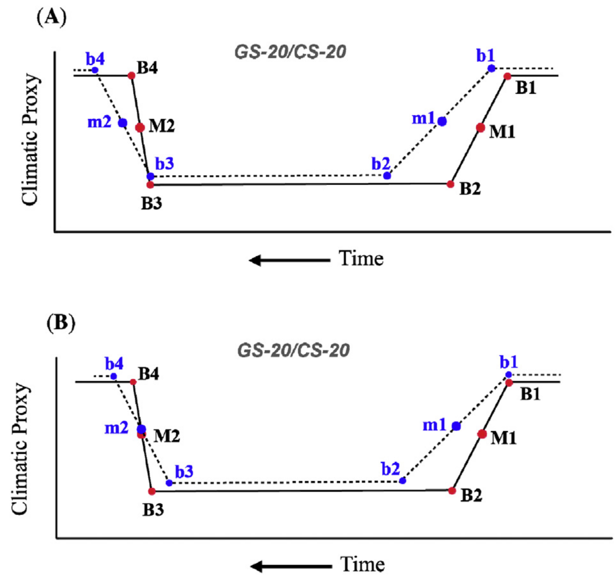

Fig. 3. Schematic of the GS-20/CS-20 events and their correlations. Conceptual $\delta^{18}O$ variations of Chinese cave (dashed line) and Greenland ice core (solid line) records across the CS-20/GS-20. B1 to B4 and b1 to b4 indicate the 'break-points' of Greenland ice core and Chinese cave $\delta^{18}O$ records, respectively. M1 and M2 and m1 and m2 depict 'mid-points' of $\delta^{18}O$ shifts in Greenland ice core and Chinese cave $\delta^{18}O$ records, respectively. Apparently, the shifts of Chinese cave $\delta^{18}O$ records into and out of the CS-20 are more gradual compared with the Greenland counterparts (GS-20). (**A**) The correlation by matching 'break-points' of b3 and B3. In this case, the initial termination shifts in both Chinese and Greenland records are assumed to be at the same time, but Greenland record reaches the new state (B4) earlier than Chinese records (b4). (**B**) The conventional correlation by matching 'mid-points' of m3 and M3. In this case, the initial shifts in Chinese records (b3) would theoretically lead the corresponding Greenland changes (B3). In addition, this correlation is virtually similar to the correlation by matching 'break-points' at the initial onset shifts (b1 and B1) (see discussions in the following text).

between the CS and GS events is coherent with the hypothesis that the trigger of millennial events resides in the northern high-latitude (e.g., Broecker, 1991, 2003; Ommen, 2015; WAIS Divide Project Members, 2015; Henry et al., 2016) (Fig. 3). Moreover, a recent work (Rosen et al., 2014) demonstrated that the abrupt temperature rise over Greenland inferred from the abrupt ice core $\delta^{18}O$ increase is nearly synchronous with or slightly leads (within 30 years) to the corresponding change in tropical methane (CH_4) sources at the onset of the Bølling–Allerød. The observation provides a critical test of the synchroneity between Greenland temperature and tropical monsoon changes. This is conceivable because AM changes as recorded by Chinese cave records can be causally linked to CH_4 variations via increases in continent rainfall and wet land expansion (e.g., Cheng et al., 2006, 2009, 2016a; Loulergue et al., 2008; Wolff, 2014; Rhodes et al., 2015, 2017). However, as a commonly-used approach, Greenland ice core records were calibrated (for example, multiplied by a factor of 1.0063) to the Hulu cave record via mid-point matching on the basis of an ambiguous assumption of contemporaneous changes in the two archives (WAIS Divide Project Members, 2015). The challenge here lies in that a number of high-resolution cave records from China reveal relatively gradual shifts in millennial-scale variations during the last glacial period that are to some extent similar to Antarctic gradual climate changes, rather than Greenland abrupt changes (e.g., Barker and Knorr, 2007; Rohling et al., 2009; Cheng et al., 2016a; Chen et al., 2016; Han et al., 2016; Zhang et al., 2016; Zhang et al., 2017). This observation thus calls for new approaches for correlating the ice core and cave records, because the conventional mid-point matching (e.g., Wang et al., 2001; Buizert et al., 2015; WAIS Divide Project Members, 2015) would imply that the initial shift in the low-latitude monsoon climate leads the

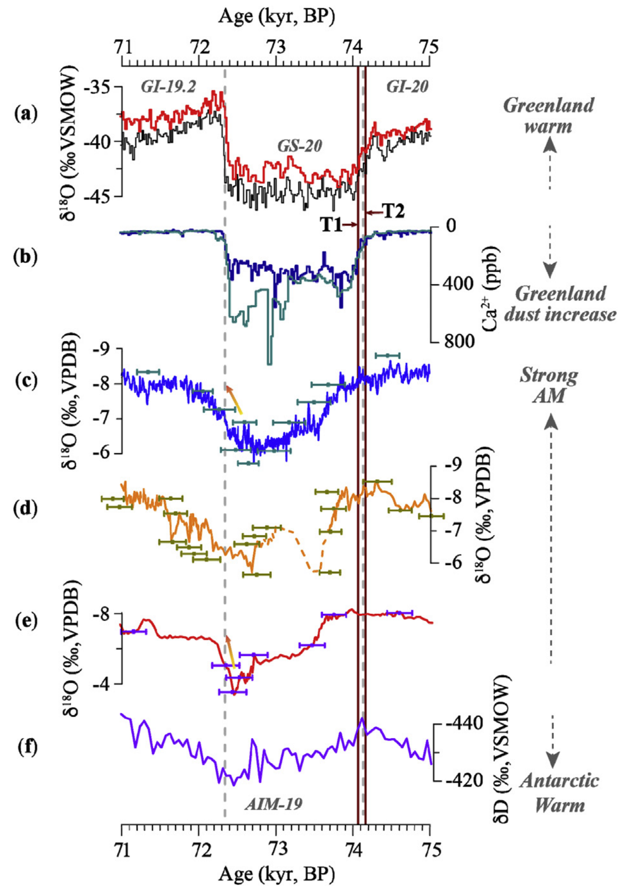

Fig. 4. Comparison of GS-20/CS-20 events. (**a**) The GS-20 in Greenland ice core NGRIP2 (black) and GISP2 (red) $\delta^{18}O$ records (GICC05modelext chronology, Seierstad et al., 2014; Rasmussen et al., 2014). (**b**) The GS-20 in the Greenland ice core NGRIP2 (blue) and GISP2 (green) [Ca^{2+}] records (GICC05modelext chronology, Seierstad et al., 2014; Rasmussen et al., 2014). (**c**)–(**e**) YK7, YK02 and WX40C $\delta^{18}O$ records, respectively (this study). (**f**) The Antarctic EDC ice core δD record (AICC02 chronology with 500 years shift to older side, Veres et al., 2013). Vertical dash lines depict the onset and termination of the GS-20 events (based on mid-points of Greenland ice core records) (Rasmussen et al., 2014). Dashed orange curve and error bars are as same as those in Fig. 2. Two vertical lines indicate the timing of the two major Toba volcanic eruptions based on the correlation to the most significant sulphate and conductivity peaks in Greenland ice core records [i.e., Toba eruptions T1 and T2 in Svensson et al. (2013)]. Orange arrows depict earlier rises in the monsoon intensity.

corresponding high-latitude temperature change due to the monsoon climate record's more gradul nature compared to the counterpart in the ice core records, thus the trigger would reside in low-latitude climate regimes (Fig. 3). This contradicts the current understanding about the climate dynamics that suggest a trigger residing at the northern high-latitude (e.g., Broecker, 1998; Stocker and Johnsen, 2003). As such, the related discussion below will focus on the correlations via the 'break-points' at either the onset or the termination of CS-20/GS-20 events, in line with the assumption of the synchroneity between the abrupt Greenland temperature change and the initial AM response (Figs. 3 and 4).

3. Results

3.1. Age model

Three stalagmite samples (YK7, YK02 and WX40C) used in this study have high U contents, allowing us to obtain high-precision ^{230}Th dates with typically 200 year uncertainty (2σ) or less. Age models were obtained by using programs Modage (Hercman and Pawlak, 2012), Stalage (Scholz and Hoffmann, 2011), Copra (Breitenbach et al., 2012), Bchron (Parnell et al., 2018), Bacon (Blaauw and Christen, 2011), and Oxcal (Ramsey, 2008), respectively (Fig. S2). The results of six age models for each stalagmite are similar to each other within uncertainties, and agree broadly with the linear interpolation results between two adjacent dates (within 95% confidence interval and the uncertainties of less than 2–3‰). We report here the Oxcal results (Table S1 and Fig. S3). The results show that the stalagmite YK7 grew fast and continuously from ~75 to 71 kyr BP (~0.03 mm/year), but slowly from ~78 to 76 kyr BP (~0.01 mm/year). YK02 shows a nearly constant growth rate of ~0.03 mm/year, but there is a hiatus from 14.7 to 15.2 cm. WX40C grew much slower with a mean growth rate of ~0.006 mm/year (Figs. S2 and S3).

3.2. Oxygen isotope records

Chinese cave $\delta^{18}O$ records have been widely used to reconstruct the AM history and its global teleconnections (e.g., Cheng et al., 2012, 2016a; 2016b). However, the climate significance of Chinese cave $\delta^{18}O$ records remains an issue in hot debate (e.g., Maher, 2008; Dayem et al., 2010; Clemens et al., 2010, 2018; Pausata et al., 2011; Caley et al., 2014; Chen et al., 2015; Liu et al., 2015; Rao et al., 2015). The disagreements stemmed at least partially from different understandings about the notion of the 'AM intensity'. Chinese cave $\delta^{18}O$ records, particularly on millennial-scale discussed here, reflect to first order changes in fraction of water vapor rained out between tropical sources and cave sites (e.g., Cheng et al., 2016a; Zhao et al., 2018): the larger atmospheric circulation, the stronger AM, the more remote moisture with more rainout along moisture trajectory, and thus the lighter cave $\delta^{18}O$ values (e.g., Yuan et al., 2004). For instance, in responding to the large millennial-scale cold events, including the CS-20/GS-20 event, cave $\delta^{18}O$ records in the AM region show a consistent heavier excursion, suggesting an overall weak AM state, although the corresponding changes in rainfall amount were likely spatially heterogeneous in the AM domain as suggested both by model simulation (e.g., LeGrande and Schmidt, 2009; Pausata et al., 2011; Liu et al., 2014) and observational data (e.g., Cheng et al., 2016b; Zhang et al., 2018). In this sense, the longstanding disparity surround the interpretation of Chinese cave $\delta^{18}O$ records is somewhat superficial rather than tangible. As such, we interpret low and high values of our cave $\delta^{18}O$ records reflecting 'stronger monsoon' and 'weaker monsoon' respectively, consistent broadly with both theoretical and empirical studies (e.g., Cheng et al., 2016a, 2016b; Zhang et al., 2018).

Our new records show a distinctive weak AM event (CS-20) with > 2‰ $\delta^{18}O$ excursion centered around 73 kyr BP (e.g., Wang et al., 2001; Cheng et al., 2006; Rasmussen et al., 2014) (Fig. 2). The structure of the event is characterized by a gradual onset (over several hundred years) and faster termination (over a few hundred years) processes in our cave records (Fig. 2). The YK7 record has the highest temporal-resolution and best age control, providing an unprecedented high-resolution (~6 years) record with much less age uncertainties across the AM CS-20 event (≤200 year dating errors, or ~140 year uncertainty based on the Oxcal age model, Fig. S3). Thus, we characterize the CS-20 event based mainly on the YK7 record, together with an additional replication test on the timing of the 'break-points' through the other two (YK02 and WX40C) records.

4. Discussion

4.1. Timing and structure of the CS-20 event

The CS-20 event in our new records has a structure characterized by a more gradual onset and termination compared to the GS-20 event in Greenland ice core records. Specifically, the onset of the GS-20 in Greenland ice core records is a relatively rapid (~300 years) cooling (inferred from a ~5‰ $\delta^{18}O$ decrease) companied by a [Ca^{2+}] (indicating dust content) increase of ~400 ppb (Fig. 4). The onset in the cave records however, show a rather gradual trend of $\delta^{18}O$ increase (> 2‰) over a ~500 year period. Intriguingly, the Antarctic EDC $\delta^{18}O$ (a temperature proxy) record also shows a gradual increase after the Greenland GS-20 onset, corresponding to the Antarctic Isotope Maxima (AIM)-19 (Svensson et al., 2013) (Fig. 4). The termination of the CS-20 event in our cave records is also relatively gradual with a $\delta^{18}O$ change of ~2‰ over apparently variable periods of ~200 (the WX40C record) to ~500 (the YK7 and YK02 records) years, yet the YK7 record is more robust due to its higher $\delta^{18}O$ temporal resolution and better dating control. The gradual changes in the cave records are noticeably similar to the Antarctic climate records (e.g., Rohling et al., 2009; Cheng et al., 2016a; Chen et al., 2016; Zhang et al., 2017), and in contrast to the abrupt changes (within ~100 years) in both Greenland temperature inferred by $\delta^{18}O$ and dust flux inferred by [Ca^{2+}] concentration (Fig. 4).

4.2. 'Break point' correlations

Our analyses show that the 'break-points' at the initial terminations of the CS-20/GS-20 events are appropriately defined in the Chinese cave and Greenland ice core $\delta^{18}O$ records (Fig. 5A). The corresponding 'break-points' in YK7, YK02 and WX40C records are at 72.6 ± 0.2, 72.4 ± 0.2, and 72.4 ± 0.2 kyr BP, respectively. The average is 72.5 kyr BP with error of about ± 200 years based directly on ^{230}Th dating error, or about ± 140 years estimated by the Oxcal age model (2σ). Accordingly, to match the 'break-points', we shift the Greenland ice core (NGRIP2 and GISP2) chronology (GICC05modelext) well within the quoted uncertainty around this time range (> 1000 years, Rasmussen et al., 2014) to older side by 150 years without changing relative ages. This suggests that the GICC05modelext chronology (after the shift of −705 years, Wolff et al., 2010) is consistent with our new correlation within ^{230}Th dating uncertainties. As a result, the termination shift in Greenland ice core records are from ~72.5 to 72.4 kyr BP with a duration of ~100 years based on the relative chronology of the ice core (Fig. 5A). Boch et al. (2011) reported a GI-19 'isotopic max. age' of 71.69 ± 0.22 (2σ) kyr BP determined from a NALPS speleothem. Consistently, this age is a few hundred years younger than 72.4 ± 0.2 kyr BP determined in this study as the onset timing of the GI-19.2. In contrast, the onset of CI-19.2 in YK7 and WX40C records are ~72.0 ± 0.2 and 72.2 ± 0.2 kyr BP, apparently lagging to the Greenland ice core records by ~200–400 years. The onset timing of the GI-19.2 in the YK02 record appears to have a longer lag to the Greenland ice core record, but less reliable than the YK7 record. On the other hand, the GS-20 onset in Greenland ice core records is from ~74.45 to 74.15 kyr BP (incorporating the 150 year shift to older side) with a duration of ~300 years (Fig. 5A). In our cave records, the corresponding 'break-points' in YK7, YK02 and WX40C records at the initial onset are ~74.1 ± 0.2, 73.9 ± 0.2 and 73.9 ± 0.2 kyr BP. The average is 74.0 kyr BP with error of about ± 200 years. There is apparently a few hundred year (or less) lag in the cave records compared to the Greenland records at the initial onset of the event, given that the uncertainty in relative age of the ice core is minor (approximately ~100 years or ~1 year/20 years across the event, Svensson et al., 2008, 2013). However, it is unclear whether the lag indicates a late AM response to the abrupt temperature change as observed in Greenland or a crucial problem stemmed from the correlation strategy itself.

Another alternative approach is the correlation via the 'break-points' at the initial onset of the CS-20/GS-20 events (the points b1 and B1 in Fig. 3). This correlation, on the basis of the YK7 'break point', will shift the Greenland records (on the GICC05modelext chronology) 150 years to younger side (within uncertainties of the ice core chronology and the ^{230}Th dating errors) (Fig. 5B). Intriguingly, this correlation sets the Greenland abrupt termination close to the middle/late of the AM termination process, and thus suggests an earlier termination shift of

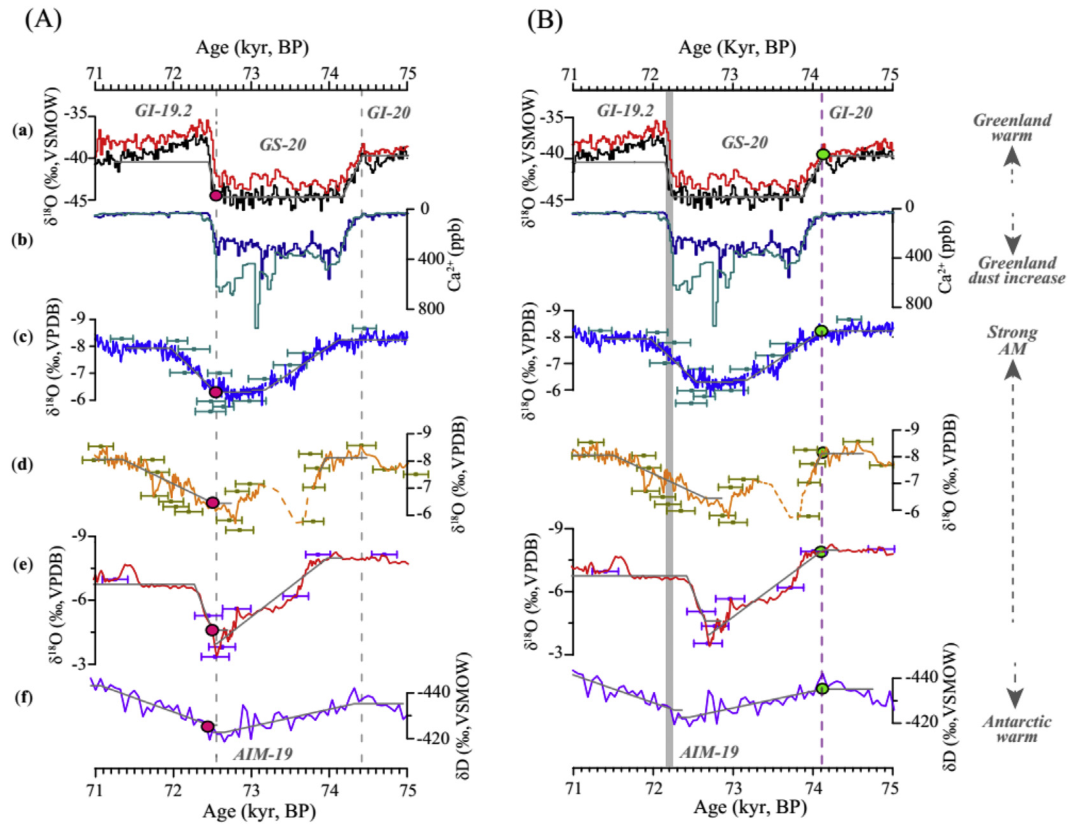

Fig. 5. The 'break-point' correlations at the initial termination (A) and onset (B) of GS/CS-20 events. Records (**a**) to (**f**) are as same as in Fig. 4. The 'break-points' were determined by the program RAMPFIT (Mudelsee, 2000). Vertical grey dash lines (A) depict the onset and termination of the GS-20 event based on the 'break-points' correlations at the initial termination. Grey bar (B) depicts the termination of the GS-20 event. Dashed orange curve and error bars are as same as in Fig. 2. Red dots (A) indicate the 'break-points' of the initial termination shift. Green dots and purple dash line (B) indicate the 'break-points' of the initial onset shift. To match the 'break-points' of the initial termination and onset shift to that in YK7 record, both YK02 and WX40C $\delta^{18}O$ records were shifted by 100 years to older side (A) and by 250 years to older side (B) respectively. The Greenland records (on the GICC05modelext chronology) were shifted by 150 years to older side (A) and by 150 years to younger side (B), respectively. The Antarctic EDC ice core δD record were shifted by 700 years (A) and 500 years (B) to older side, respectively.

the CS-20 event (Fig. 5B). In other words, regarding climatic dynamics, while the initial onset of the GS-20/CS-20 events are presumed to be synchronous, the CS-20 event termination should start a few hundred years earlier in the low-latitude climate regime compared with the Greenland GS-20 event.

4.3. Global correlations

The structures of the CS-20 event in our records are similar to other Chinese cave records with lower resolutions (Fig. 6). In addition, a cave $\delta^{18}O$ record from northern Borneo, Malaysia also shows a similar hydroclimatic transition in the tropical region centered at ~73.4 kyr BP (Carolin et al., 2013). Recent $\delta^{18}O$ data from Qal'e Kord cave, Iran reveals a drying event in the Asian Westerly climate region, equivalent to the CS-20/GS-20 (Mehterian et al., 2017). In the South American Monsoon (SAM) regime in Southern Hemisphere, the GS-20 event is an anti-phased hydroclimatic excursion (relative to the AM) in $\delta^{18}O$ records from Botuverá (Cruz et al., 2005; Wang et al., 2006) and Cueva del Diamante (Cheng et al., 2013a) caves. In addition, based on our correlations, the two possible Toba volcanic eruptions [T1 and T2 defined in Svensson et al. (2013)] occured at ~74.21 and 74.31 kyr BP according to the correlation via the 'break points' of the initial termination (Fig. 6A) or at 73.91 and 74.01 kyr BPaccording to the correlation via the 'break points' of the initial onset (Fig. 6B), coincided with a previous determination of 73.88 ± 0.64 kyr BP (2σ, full external errors, Storey et al., 2012). In comparison with the Chinese cave records, these two volcanic events occurred around the initial onset of the AM reduction (Fig. 6), suggesting a possible link between the Toba eruption and the largest AM reduction during the last glacial period.

4.4. Underlying dynamics

The 'break-point' correlations between Chinese cave and Greenland ice core $\delta^{18}O$ records (Figs. 3 and 5) is likely an appropriate approach, because it underlines that their initial changes occurred at the same time. As aforementioned, such correlations are consistent with a synchronous or slightly leading relationship between Greenland and tropical changes on millennial-scale (i.e., 4.5 + 21/-24 years, Rosen et al., 2014; Wolff, 2014). On the other hand, the more gradual monsoon shifts afterwards in comparison with the abrupt Greenland temperature change are likely attributed to an important role of ocean circulation and/or sea surface temperature in reorganizations of low–latitude climate (WAIS Divide Project Members, 2015). The gradual shifts of the monsoon responses take a few hundred years longer than Greenland temperature changes (Fig. 5), which is of the same order compared to the observed lag (~200 years) of the Antarctic responses to the northern high-latitude changes due to a central role of ocean circulations (WAIS Divide Project Members, 2015). In principle, the monsoon variability is largely driven by the temperature gradient between land and ocean, and hence it is expected that the corresponding monsoon changes would take longer time because of relatively slow responses of oceanic processes to the abrupt climate change recorded in Greenland ice core records.

Two decades ago, a mechanism of the bipolar seesaw was proposed to explain the anti-phase temperature variance between Greenland and Antarctica (e.g., Broecker, 1998; Stocker, 1998). According to this

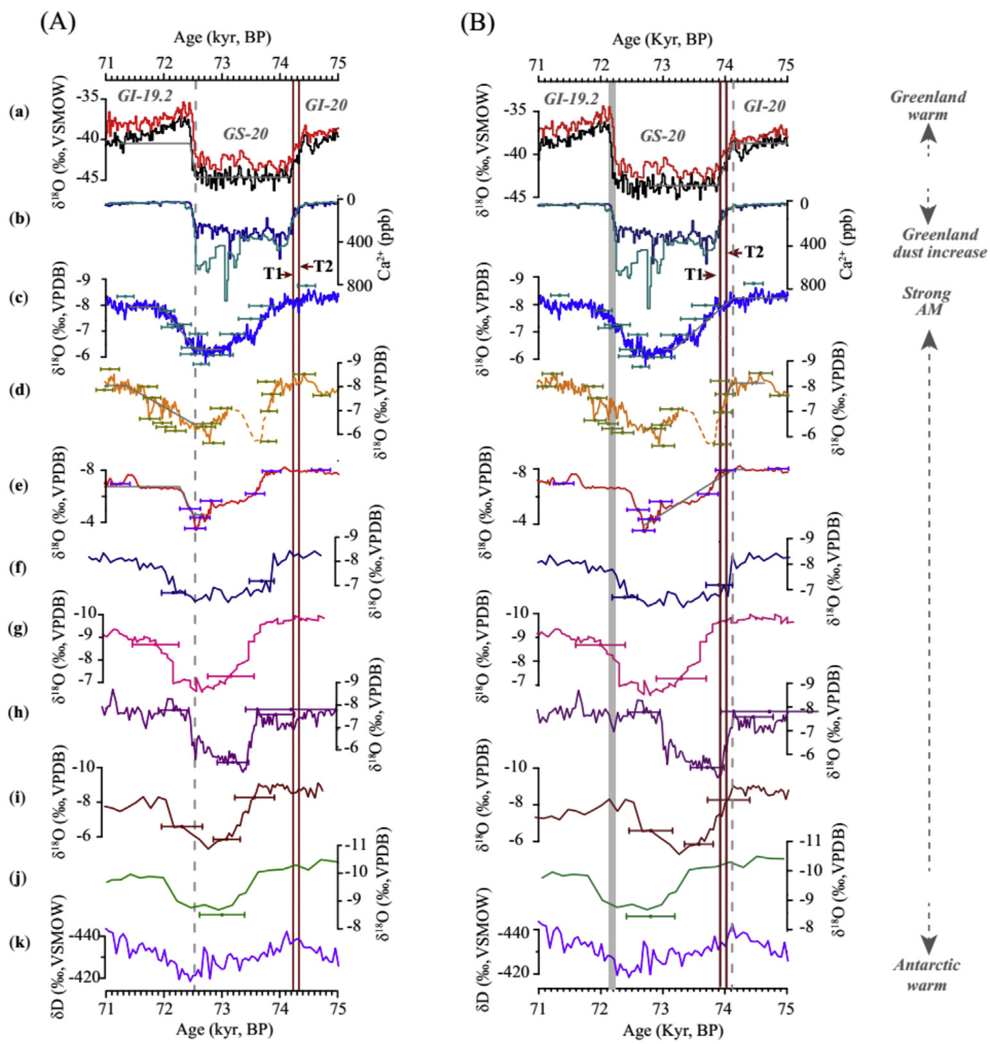

Fig. 6. The correlations of the GS-20/CS-20 events at the initial termination (A) and onset (B) 'break-points'. (**a**) Greenland ice core NGRIP2 (black) and GISP2 (red) $\delta^{18}O$ records. (**b**) The GS-20 in the Greenland ice core NGRIP2 (blue) and GISP2 (green) [Ca^{2+}] records. The ice core chronologies are based on GICC05modelext (Seierstad et al., 2014; Rasmussen et al., 2014) with 150 year shift to older side (A) and 150 years to younger side (B). (**c**)–(**e**) YK7, YK02 and WX40C $\delta^{18}O$ records respectively (this study) [YK02 and WX40C records shifted by 100 years (A) and 250 years (B) to older side to match the 'breakpoint' of the initial termination and onset in the YK7 record respectively]. (**f**)–(**i**) Chinese cave $\delta^{18}O$ records: the JFYK7 record from Yangkou cave (with ~600 year (A) and ~850 year (B) shifts to older side) (Zhang et al., 2017), SB22 record from Sanbao cave (with ~400 year (A) and ~600 year (B) shifts to older side) (Wang et al., 2008), the MSL record from Hulu cave (with ~250 year (A) and ~800 year (B) shifts to older side), and the YX46 record from Yongxing cave (with ~150 year (A) and ~600 year (B) shifts to older side) (Chen et al., 2016), respectively. (**j**) The SC03 $\delta^{18}O$ record from Secret cave, Borneo, Malaysia (with 400 year (A) and ~200 year (B) shifts to older side) (Carolin et al., 2013). (**k**) The EDC ice core δD record (the AICC02 chronology with 500 year shifts to older side, Veres et al., 2013). The age shifts are within or around the margin of the maximum shifts that one could possibly make according to original dating results, $\delta^{18}O$ temporal resolutions, and the uncertainties in choice of 'break point'. Further work is clearly needed to assess the shifts and in turn the correlations. Vertical grey dash lines depict the correlation of the initial termination (A) and onset (B) of the GS-20/CS events between different records. Grey bar depict the termination of the GS-20 event (B). Two vertical lines indicate the timing of the Toba volcanic eruptions based on its correlation to the most significant sulphate and conductivity peaks in Greenland ice core records [i.e., Toba eruptions T1 and T2 in Svensson et al. (2013)]. Dashed orange curves and error bars are as same as in Fig. 2.

hypothesis, changes in the Atlantic meridional overturning circulation (AMOC) was a key process that explains millennial-scale climate oscillations during the last glacial period, including the GS-20 event (e.g., Broecker and Denton, 1989; Alley, 2007; Cosford et al., 2008; Cheng et al., 2012; Stocker and Johnsen, 2003; Wolff, 2014): a shut-off/slowdown (or reinitiating) of the AMOC, triggering rapid cooling (or warming) in the north, should cause a warming (cooling) in the south, and vice versa. The observed Antarctic temperature variations inferred by δD records from Antarctic ice cores show more gradual responses (e.g., Veres et al., 2013) with a lag (~200 ± 100 years) to the Greenland changes (WAIS Divide Project Members, 2015), consistent with the bipolar seesaw hypothesis. This mechanism may explain the wide anti-phased relationship of millennial events between north and south as well, including the global monsoon variations (e.g., Cheng et al., 2012) (Fig. 6). In addition, the corresponding variations of the low-latitude monsoons inferred by cave records behave indeed a pattern between Greenland and Antarctica: more gradual than Greenland, but more abrupt than Antarctica (Figs. 4–6). It thus appears that the monsoonal variations on millennial-scale may be suited in a response framework coherent with the bipolar seesaw mechanism.

The correlation between the Chinese AM and Greenland temperature records involves the climatic dynamics outlined above, which has not been cautiously considered in the past. With considerable improvements in both proxy resolution and dating precision, it is now necessary and possible as well to reexamine the strategies of correlation between the Chinese and Greenland records. The conventional mid-point correlation would suggest an earlier low-latitude monsoonal change than abrupt Greenland temperature jump (Fig. 3). Additionally, regarding the GS-20/CS-20 events, only one of mid-points, either onset or termination, can be correlated because of the shorter CS-20 duration between the two mid-points compared with the GS-20 (Figs. 3–5). The correlation via the 'break points' at the initial termination shift (Fig. 3A) would imply a synchronous termination of the GS-20/CS-20 events with the trigger likely resided in the northern high-latitude. According to this correlation, however, the CS-20 onset would lag to the GS-20 by a few hundred years (Figs. 3–5). Alternatively, The correlation via the 'break points' at the initial onset shift would imply a synchronous onset of the GS-20/CS-20 events with the trigger also likely resided in the northern high-latitude. However, this correlation would also imply that GS-20 termination lag to the CS-20 by a few hundred years, similar to the results from the mid-point matching strategy (Figs. 3–5).

Whether the above approaches via 'break-point' correlations are valid remain an open question, which is largely dependent on our understating about the underlying climate dynamics, and beyond the scope of this study. Instead, with our new high-resolution and precisely dated Chinese cave records, we now can demonstrate different approaches to the correlation between AM and Greenland temperature records in the context of their underlying climatic dynamics. Nevertheless, more high-resolution and precisely dated climate records and model simulations are critical in order to better understand the mechanism behind the millennial climate events and in turn to attain an appropriate correlation between the Chinese AM and Greenland temperature changes.

5. Conclusions

Three new Chinese cave $\delta^{18}O$ records characterize the AM variations across the CS-20 event in detail. In all records, the event has common (within error) 'break-points' at 72.5 ± 0.2 and ~74.0 ± 0.2 kyr BP, marking the initial termination and onset shifts, respectively. The two timing-benchmarks are used respectively to correlate the similar 'break-points' in Greenland ice core $\delta^{18}O$ records, suggesting an ice core chronology (GICC05modelext) shift of ~150 years to older and younger side, accordingly. While both shifts inferred by the two different correlations are well within the current uncertainty of the ice core chronology across the time range, their underlying climate dynamics are quite different. On the basis of the correlation via the initial termination shifts, the more gradual termination of the CS-20 event in the cave records suggest a few hundred year lag of complete monsoon responses to the abrupt change in Greenland ice core records. This lag is comparable in terms of duration with that of Antarctic temperature response (WAIS Divide Project Members, 2015), suggesting a key role of oceanic reorganizations in the propagation of the abrupt climate signal presumably originated in northern high-latitude (or the North Atlantic). On the other hand, on the basis of the correlation via the initial onset shifts, the initial termination shift of the CS-20 leads the GS-20 termination by a few hundred years, implying a more important and active role of the low-latitude climate change in driving millennial-scale climate variations. The different correlations and their different climatic dynamics call for further observational and modeling studies.

Acknowledgments

This work is supported by grants from National Natural Science Foundation of China to H.C. (NSFC 41731174, 41888101, 41561144003 and 4157020432), US National Science Foundation 1702816 to R.L.E and H.C., National Natural Science Foundation of China to P.Z.Z. (NSFC 41473009 and 41273014), and X.L.Y. (NSFC 41572158 and 41272192).

Appendix B. Supplementary data

Supplementary data to this article can be found online at https://doi.org/10.1016/j.quageo.2019.05.002.

Appendix A. Supplementary material

Supplementary data related to this article can be found online.

References

Adolphi, F., Ramsey, C.B., Erhardt, T., Edwards, R.L., Cheng, H., Turney, M., Cooper, A., Svensson, A., Rasmussen, O.S., Fischer, H., Muscheler, R., 2018. Connecting the Greenland ice-core and U-Th timescales via cosmogenic radionuclides: testing the synchroneity of Dansgaard–Oeschger events. Clim. Past 14, 1755–1781.
Alley, R.B., 2007. Wally was right: predictive ability of the north atlantic "conveyor belt" hypothesis for abrupt climate change. Annu. Rev. Earth Planet Sci. 35 (1), 241–272.
Andersen, K.K., Svensson, A., Johnsen, S.J., Rasmussen, S.O., Bigler, M., Röthlisberger, R., Ruth, U., Siggaard-Andersen, M., Peder Steffensen, J., Dahl-Jensen, D., 2006. The Greenland Ice Core Chronology 2005, 15–42ka. Part 1: constructing the time scale. Quat. Sci. Rev. 25 (23–24), 3246–3257.
Barker, S., Knorr, G., 2007. From the Cover: Antarctic climate signature in the Greenland ice core record. Proc. Natl. Acad. Sci. U.S.A. 104 (44), 17278–17282.
Blaauw, M., Christen, J.A., 2011. Flexible paleoclimate age-depth models using an autoregressive gamma process. Bayesian Analy 6 (3), 457–474.
Blockley, S.P.E., Lane, C.S., Hardiman, M., Rasmussen, S.O., Seierstad, I.K., Steffensen, J.P., Svensson, A., Lotter, A.F., Turney, C.S.M., Bronk Ramsey, C., 2012. Synchronisation of palaeoenvironmental records over the last 60,000 years, and an extended INTIMATE event stratigraphy to 48,000 b2k. Quat. Sci. Rev. 36, 2–10.
Boch, R., Cheng, H., Spötl, C., Edwards, R.L., Wang, X.F., Häuselmann, Ph, 2011. A precisely dated European climate proxy stack 120-60 ka. Clim. Past Discss. 7, 1049–1072.
Breitenbach, S.F.M., Rehfeld, K., Goswami, B., Baldini, J.U.L., Ridley, H.E., Kennett, D.J., Prufer, K.M., Aquino, V.V., Asmerom, Y., Polyak, V.J., Cheng, H., Kurths, J., Marwan, N., 2012. Constructing Proxy Records from Age models (COPRA). Clim. Past 8 (5), 1765–1779.
Broecker, W.S., 1991. The great conveyer belt. Oceanography 4, 79–89.
Broecker, W.S., 1998. Paleocean circulation during the last deglaciation: a bipolar seesaw? Paleoceanography 13 (2), 119–121.
Broecker, W.S., 2003. Does the trigger for abrupt climate change reside in the ocean or in the atmosphere? Science 300 (5625), 1519–1522.
Broecker, W.S., Denton, G.H., 1989. The role of ocean-atmosphere reorganizations in glacial cycles. Geochem. Cosmochim. Acta 53, 2465–2501.
Buizert, C., Cuffey, K.M., Severinghaus, J.P., Baggenstos, D., Fudge, T.J., Steig, E.J., Markle, B.R., Winstrup, M., Rhodes, R.H., Brook, E.J., Sowers, T.A., Clow, G.D., Cheng, H., Edwards, R.L., Sigl, M., McConnell, J.R., Taylor, K.C., 2015. The WAIS Divide deep ice core WD2014 chronology- Part 1: methane synchronization (68–31 ka BP) and the gas age–ice age difference. Clim. Past 11 (2), 153–173.
Caley, T., Roche, D.M., Renssen, H., 2014. Orbital Asian summer monsoon dynamics revealed using an isotope-enabled global climate model. Nat. Commun. 5, 5371.
Carolin, S.A., Cobb, K.M., Adkins, J.F., Clark, B., Conroy, J.L., 2013. Varied response of western Pacific hydrology to climate forcings over the last glacial period. Science 340 (6140), 1564–1566.
Chen, S., Wang, Y., Cheng, H., Edwards, R.L., Wang, X., Kong, X., Liu, D., 2016. Strong coupling of Asian Monsoon and Antarctic climates on sub-orbital timescales. Sci. Rep. 6 (1), 1–7.
Chen, F.H., Xu, Q.H., Chen, J.H., Birks, H.J.B., Liu, J.B., Zhang, S.R., Jin, L.Y., An, C.B., Telford, R.J., Cao, X.Y., Wang, Z.L., Zahng, X.J., Selvaraj, K., Lü, H.Y., Li, Y.C., Zheng, Z., Wang, H.P., Zhou, A.F., Dong, G.H., Zhang, J.W., Huang, X.Z., Bloemendal, J., Rao, Z.G., 2015. East Asian summer monsoon precipitation variability since the last deglaciation. Sci. Rep. 5 (1), 11186.
Cheng, H., Edwards, R.L., Hoff, J., Gallup, C.D., Richards, D.A., Asmerom, Y., 2000. The half-life of uranium-234 and thorium-230. Chem. Geol. 169, 17–33.
Cheng, H., Edwards, R.L., Wang, Y., Kong, X., Ming, Y., Kelly, M.J., Wang, X., Gallup, C.D., 2006. A penultimate glacial monsoon record from Hulu Cave and two-phase glacial terminations. Geology 3 (34), 217–220.
Cheng, H., Edwards, R.L., Broecker, W.S., Denton, G.H., Kong, X., Wang, Y., Zhang, R., Wang, X., 2009. Ice age terminations. Science 326 (5950), 248–252.
Cheng, H., Edwards, R.L., Sinha, A., Spötl, C., Yi, L., Chen, S., Kelly, M., Kathayat, G., Wang, X., Li, X., Kong, X., Wang, Y., Ning, Y., Zhang, H., 2016a. The Asian monsoon over the past 640,000 years and ice age terminations. Nature 534 (7609), 640–646.
Cheng, H., Lawrence Edwards, R., Shen, C., Polyak, V.J., Asmerom, Y., Woodhead, J., Hellstrom, J., Wang, Y., Kong, X., Spötl, C., Wang, X., Calvin Alexander, E., 2013a. Improvements in ^{230}Th dating, ^{230}Th and ^{234}U half-life values, and U–Th isotopic measurements by multi-collector inductively coupled plasma mass spectrometry. Earth Planet. Sci. Lett. 371–372, 82–91.
Cheng, H., Sinha, A., Cruz, F.W., Wang, X., Edwards, R.L., D Horta, F.M., Ribas, C.C., Vuille, M., Stott, L.D., Auler, A.S., 2013b. Climate change patterns in Amazonia and biodiversity. Nat. Commun. 4 (1), 1411.
Cheng, H., Sinha, A., Wang, X., Cruz, F.W., Edwards, R.L., 2012. The global paleomonsoon as seen through speleothem records from asia and the americas clim. Dynamis 39 (5), 1045–1062.
Cheng, H., Spötl, C., Breitenbach, S.F., Sinha, A., Wassenburg, J.A., Jochum, K.P., Scholz, D., Li, X., Yi, L., Peng, Y., Lv, Y., Zhang, P., Votintseva, A., Loginov, V., Ning, Y., Kathayat, G., Edwards, R.L., 2016b. Climate variations of Central Asia on orbital to millennial timescales. Sci. Rep. 6, 36975.
Cheng, H., Edwards, R.L., Southon, J., Matsumoto, K., Feinberg, M.J., Sinha, A., Zhou, W.J., Li, H.Y., Li, X.L., Xu, Y., Chen, S.T., Tan, M., Wang, Q., Wang, Y.J., Ning, Y.F., 2018. Atmospheric $^{14}C/^{12}C$ changes during the last glacial period from Hulu Cave. Science 362 (6420), 1293–1297.
Clemens, S.C., Prell, W.L., Sun, Y.B., 2010. Orbital-scale timing and mechanisms driving Late Pleistocene Indo-Asian summer monsoons: reinterpreting cave speleothem $\delta^{18}O$. Paleoceanograpgy 25, 4207.
Clemens, S.C., Holbourn, A., Kubota, Y., Lee, K.E., Liu, Z., Chen, G., Nelson, A., Fox-Kemper, B., 2018. Precession-band variance missing from East Asian monsoon run off. Nat. Commun. 9, 3364.
Cosford, J., Qing, H., Yuan, D., Zhang, M., Holmden, C., Patterson, W., Hai, C., 2008. Millennial-scale variability in the Asian monsoon: evidence from oxygen isotope records from stalagmites in southeastern China. Palaeogeogr. Palaeoclimatol. Palaeoecol. 266 (1–2), 3–12.
Cruz, F.W., Burns, S.J., Karmann, I., Sharp, W.D., Vuille, M., Cardoso, A.O., Ferrarl, J.A., Silva, P.L., Viana, O., 2005. Insolation-driven changes in atmospheric circulation over the past 116,000 years in subtropical Brazil. Nature 434 (7029), 63–66.
Dansgaard, W., Johnsen, S.J., Clausen, H.B., Dahl-Jensen, D., Steffensen, J.P., Jouzel, J., Johnsen, S.J., Hvidberg, C.S., Gundestrup, N.S., Hammer, C.U., Dansgaard, W., Clausen, H.B., Sveinbj Rnsdottir, A.E., Bond, G., 1993. Evidence for general instability of past climate from a 250-kyr ice-core record. Nature 364 (6434), 218–220.
Dayem, K.E., Molnar, P., Battisti, D.S., Roe, G.H., 2010. Lessons learned from oxygen isotopes in modern precipitation applied to interpretation of speleothem records of paleoclimate from eastern Asia. Earth Planet. Sci. Lett. 295 (1–2), 219–230.
Edwards, R.L., Chen, J.H., Wasserburg, G.J., 1987. ^{238}U, ^{234}U, ^{230}Th, ^{232}Th systematics

and the precise measurement of time over the past 500,000 years. Earth Planet. Sci. Lett. 81 (2), 175–192.
Fleitmann, D., Burns, S.J., Mudelsee, M., Neff, U., Kramers, J., Mangini, A., Matter, A., 2003. Holocene forcing of the Indian monsoon recorded in a stalagmite from southern Oman. Science 300 (5626), 1737–1739.
Han, L., Li, T., Cheng, H., Edwards, R.L., Shen, C., Li, H., Huang, C., Li, J., Yuan, N., Wang, H., Zhang, T., Zhao, X., 2016. Potential influence of temperature changes in the Southern Hemisphere on the evolution of the Asian summer monsoon during the last glacial period. Quat. Int. 392, 239–250.
Haslam, M., Petraglia, M., 2010. Environmental impact of the 73ka Toba super-eruption in South asia. Comment on Williams, M.A.J., Ambrose, S.H., van der Kaars, S., Ruehlemann, C., Chattopadhyaya, U., Pal, J., Chauhan, P.R. (Eds.), [Palaeogeography, Palaeoclimatology, Palaeoecology 284 (2009) 295–314]. Palaeogeo. Palaeocli. Palaeoeco. 296 (1–2), 199–203.
Hercman, H., Pawlak, J., 2012. MOD-AGE: An age-depth model construction algorithm. Quat. Geochronol 12, 1–10.
Henderson, G.M., 2006. Caving in to new chronologies. Science 313 (5787), 620–622.
Henry, L.G., McManus, J.F., Curry, W.B., Roberts, N.L., Piotrowski, A.M., Keigwin, L.D., 2016. North Atlantic ocean circulation and abrupt climate change during the last glaciation. Science 353 (6298), 470–473.
Johnsen, S.J., Dahl-Jensen, D., Gundestrup, N., Steffensen, J.P., Clausen, H.B., Miller, H., Masson-Delmotte, V., Sveinbjörnsdottir, A.E., White, J., 2001. Oxygen isotope and palaeotemperature records from six Greenland ice-core stations: camp Century, Dye-3, GRIP, GISP2, Renland and NorthGRIP. J. Quat. Sci. 16 (4), 299–307.
Jiang, X.Y., He, Y.Q., Shen, C.-C., Kong, X.G., Zhong, L.Z., Chang, Y.W., 2012. Stalagmite-inferred holocene precipitation in northern guizhou province, China, and asynchronous termination of the climatic optimum in the asian monsoon territory. Chin. Sci. Bull. 57 (7), 795–801.
LeGrande, A.N., Schmidt, G.A., 2009. Sources of Holocene variability of oxygen isotopes in paleoclimate archives. Clim. Past 5, 441–455.
Li, T., Shen, C., Huang, L., Jiang, X., Yang, X., Mi, H., Lee, S.Y., Lo, L., 2014. Stalagmite-inferred variability of the Asian summer monsoon during the penultimate glacial–interglacial period. Clim. Past 10 (3), 1211–1219.
Liu, J.B., Chen, J.,H., Zhang, X.J., Li, Y., Rao, Z.G., Chen, F.H., 2015. Holocene East Asian summer monsoon records in northern China and their inconsistency with Chinese stalagmite $\delta^{18}O$ records. Earth Sci. Rev. 148, 194–208.
Liu, Z., Wen, X., Brady, E.C., Otto-Bliesner, B., Yu, G., Lu, H., Cheng, H., Wang, Y., Zhang, W., Ding, Y., Edwards, R.L., Cheng, J., Liu, W., Yang, H., 2014. Chinese cave records and the east asia summer monsoon. Quat. Sci. Rev. 83, 115–128.
Loulergue, L., Schilt, A., Spahni, R., Masson-Delmotte, V., Blunier, T., Lemieux, B., Barnola, J., Raynaud, D., Stocker, T.F., Chappellaz, J., 2008. Orbital and millennial-scale features of atmospheric CH_4 over the past 800,000 years. Nature 453 (7193), 383–386.
Maher, B.A., 2008. Holocene variability of the East Asian summer monsoon from Chinese cave records: a reassessment. Holocene 18, 861–866.
Mehterian, S., Pourmand, A., Sharifi, A., Lahijani, H.A.K., Naderi, M., Swart, P.K., 2017. Speleothem records of glacial/interglacial climate from Iran forewarn of future Water Availability in the interior of the Middle East. Quat. Sci. Rev. 164, 187–198.
Mudelsee, M., 2000. Ramp function regression: a tool for quantifying climate transitions. Comput. Geosci. 26 (3), 293–307.
North Greenland Ice Core Project members, 2004. High-resolution record of Northern Hemisphere climate extending into the last interglacial period. Nature 431 (7005), 147–151.
Ommen, T.V., 2015. Northern push for the bipolar see-saw. Nature 520, 630–631.
Parnell, A.C., Haslett, J., Allen, J.R.M., Buck, C.E., Huntley, B., 2018. A flexible approach to assessing synchroneity of past events using Bayesian reconstructions of sedimentation history. Quat. Sci. Rev. 27, 1872–1885.
Pausata, F.S.R., Battisti, D.S., Nisancioglu, K.H., Bitz, C.M., 2011. Chinese stalagmite $\delta^{18}O$ controlled by changes in the Indian monsoon during a simulated Heinrich event. Nat. Geosci. 4, 474–480.
Rampino, M.R., Self, S., 1992. Volcanic winter and accelerated glaciation following the Toba super-eruption. Nature 359 (6390), 50–52.
Ramsey, C.B., 2008. Deposition models for chronological records. Quat. Sci. Rev. 27 (1), 42–60.
Rao, Z.G., Liu, X.K., Hua, H., Gao, Y.L., Chen, F.H., 2015. Evolving history of the East Asian summer monsoon intensity during the MIS5: inconsistent records from Chinese stalagmites and loess deposits. Environ. Earth Sci. 73 (7), 3937–3950.
Rasmussen, S.O., Andersen, K.K., Svensson, A.M., Steffensen, J.P., Vinther, B.M., Clausen, H.B., Siggaard-Andersen, M.L., Johnsen, S.J., Larsen, L.B., Dahl-Jensen, D., Bigler, M., Thlisberger, R.R., Fischer, H., Goto-Azuma, K., Hansson, M.E., Ruth, U., 2006. A new Greenland ice core chronology for the last glacial termination. J. Geophys. Res. 111 (D6), 907–923.
Rasmussen, S.O., Bigler, M., Blockley, S.P., Blunier, T., Buchardt, S.L., Clausen, H.B., Cvijanovic, I., Dahl-Jensen, D., Johnsen, S.J., Fischer, H., Gkinis, V., Guillevic, M., Hoek, W.Z., Lowe, J.J., Pedro, J.B., Popp, T., Seierstad, I.K., Steffensen, J.P., Svensson, A.M., Vallelonga, P., Vinther, B.M., Walker, M.J.C., Wheatley, J.J., Winstrup, M., 2014. A stratigraphic framework for abrupt climatic changes during the Last Glacial period based on three synchronized Greenland ice-core records: refining and extending the INTIMATE event stratigraphy. Quat. Sci. Rev. 106, 14–28.
Rhodes, R.H., Brook, E.J., Chiang, J.C.H., Blunier, T., Maselli, O.J., McConnell, J.R., Romanini, D., Severinghaus, J.P., 2015. Enhanced tropical methane production in response to iceberg discharge in the North Atlantic. Science 348 (6238), 1016–1019.
Rhodes, R.H., Brook, E.J., McConnell, J.R., Blunier, T., Sime, L.C., Faïn, X., Mulvaney, R., 2017. Atmospheric methane variability: centennial-scale signals in the last glacial period. Glob. Biogeochem. Cycles 31 (3), 575–590.
Rohling, E.J., Liu, Q.S., Roberts, A.P., Stanford, J.D., Rasmussen, S.O., Langen, P.L., Siddall, M., 2009. Controls on the East Asian monsoon during the last glacial cycle, based on comparison between Hulu Cave and polar ice-core records. Quat. Sci. Rev. 28 (27), 3291–3302.
Rousseau, D., Boers, N., Sima, A., Svensson, A., Bigler, M., Lagroix, F., Taylor, S., Antoine, P., 2017. (MIS3 & 2) millennial oscillations in Greenland dust and Eurasian aeolian records- A paleosol perspective. Quat. Sci. Rev. 169, 99–113.
Rosen, J.L., Brook, E.J., Severinghaus, J.P., Blunier, T., Mitchell, L.E., Lee, J.E., Edwards, J.S., Gkinis, V., 2014. An ice core record of near-synchronous global climate changes at the Bolling transition. Nat. Geosci. 7, 459–463.
Scholz, D., Hoffmann, D.L., 2011. StalAge- An algorithm designed for construction of speleothem age models. Quat. Geochronol 6, 369–382.
Seierstad, I.K., Abbott, P.M., Bigler, M., Blunier, T., Bourne, A.J., Brook, E., Buchardt, S.L., Buizert, C., Clausen, H.B., Cook, E., Dahl-Jensen, D., Davies, S.M., Guillevic, M., Johnsen, S.J., Pedersen, D.S., Popp, T.J., Rasmussen, S.O., Severinghaus, J.P., Svensson, A., Vinther, B.M., 2014. Consistently dated records from the Greenland GRIP, GISP2 and NGRIP ice cores for the past 104ka reveal regional millennial-scale $\delta^{18}O$ gradients with possible Heinrich event imprint. Quat. Sci. Rev. 106, 29–46.
Shen, C.-C., Edwards, R.L., Cheng, H., Dorale, J.A., Thomas, R.B., Moran, S.B., Weinstein, S.E., Edmonds, H.N., 2002. Uranium and thorium isotopic and concentration measurements by magnetic sector inductively coupled plasma mass spectrometry. Chem. Geol. 185 (3–4), 165–178.
Shen, C.-C., Cheng, H., Edwards, R.L., Moran, S.B., Edmonds, H.N., Hoff, J.A., Thomas, R.B., 2003. Measurement of attogram quantities of ^{231}Pa in dissolved and particulate fractions of seawater by isotope dilution thermal ionization mass spectroscopy. Anal. Chem. 75 (5), 1075–1079.
Spötl, C., Mattey, D., 2006. Stable isotope microsampling of speleothems for palaeoenvironmental studies: a comparison of microdrill, micromill and laser ablation techniques. Chem. Geol. 235 (1–2), 48–58.
Steffensen, J.P., Andersen, K.K., Bigler, M., Clausen, H.B., Jensen, D.D., Fischer, H., Azuma, K.,G., Hansson, M., Johnsen, S.J., Jouzel, J., Delmotte, V.M., Popp, T., Rasmussen, S.O., Röthlisberger, R., Ruth, U., Stauffer, B., Andersen, M.L.S., Sverinbjörnsdóttir, A.E., Svensson, A., White, J.W.C., 2008. High-resolution Greenland ice core data show abrupt climate change happens in few years. Science 321 (5889), 680–683.
Stocker, T.F., 1998. The seesaw effect. Science 282, 61–62.
Stocker, T.F., Johnsen, S.J., 2003. A minimum thermodynamic model for the bipolar seesaw. Paleoceanography 18 (4), 1087.
Storey, M., Roberts, R.G., Saidin, M., 2012. Astronomically calibrated 40Ar/39Ar age for the Toba supereruption and global synchronization of late Quaternary records. Proc. Natl. Acad. Sci. U.S.A. 109 (46), 18684–18688.
Svensson, A., Andersen, K.K., Bigler, M., Clausen, H.B., Jensen, D.D., Davies, S.M., Johnsen, S.J., Muscheler, R., Parrenin, F., Rasmussen, S.O., Rothlisberger, R., Seierstad, I., Steffensen, J.P., Vinther, B.M., 2008. A 60000 year Greenland stratigraphic ice core chronology. Clim. Past 4, 47–57.
Svensson, A., Bigler, M., Blunier, T., Clausen, H.B., Dahl-Jensen, D., Fischer, H., Fujita, S., Goto-Azuma, K., Johnsen, S.J., Kawamura, K., Kipfstuhl, S., Kohno, M., Parrenin, F., Popp, T., Rasmussen, S.O., Schwander, J., Seierstad, I., Severi, M., Steffensen, J.P., Udisti, R., Uemura, R., Vallelonga, P., Vinther, B.M., Wegner, A., Wilhelms, F., Winstrup, M., 2013. Direct linking of Greenland and Antarctic ice cores at the Toba eruption (74 kyr BP). Clim. Past 9, 749–766.
Veres, D., Bazin, L., Landais, A., Toyé Mahamadou Kele, H., Lemieux-Dudon, B., Parrenin, F., Martinerie, P., Blayo, E., Blunier, T., Capron, E., Chappellaz, J., Rasmussen, S.O., Severi, M., Svensson, A., Vinther, B., Wolff, E.W., 2013. The Antarctic ice core chronology (AICC2012): an optimized multi-parameter and multi-site dating approach for the last 120 thousand years. Clim. Past 9 (4), 1733–1748.
Vinther, B.M., Clausen, H.B., Johnsen, S.J., Rasmussen, S.O., Andersen, K.K., Buchardt, S.L., Dahl-Jensen, D., Seierstad, I.K., Siggaard-Andersen, M.L., Steffensen, J.P., Svensson, A., Olsen, J., Heinemeier, J., 2006. A synchronized dating of three Greenland ice cores throughout the Holocene. J Geophy. Res. Atmos. 111 (D13), 2581–2591.
WAIS Divide Project Members, 2015. Precise interpolar phasing of abrupt climate change during the last ice age. Nature 520 (7549), 661–665.
Wang, X., Auler, A.S., Edwards, R.L., Cheng, H., Ito, E., Solheid, M., 2006. Interhemispheric anti-phasing of rainfall during the last glacial period. Quat. Sci. Rev. 25 (23–24), 3391–3403.
Wang, Y., Cheng, H., Edwards, R.L., Kong, X., Shao, X., 2008. Millennial- and orbital-scale changes in the East Asian monsoon over the past 224,000 years. Nature 451 (7182), 1090–1093.
Wang, Y.J., Cheng, H., Edwards, R.L., An, Z.S., Wu, J.Y., Shen, C.C., Dorale, J.A., 2001. A high-resolution absolute-dated late pleistocene monsoon record from Hulu cave, China. Nature 294 (5550), 2345–2348.
Williams, M.A.J., Ambrose, S.H., der Kaars, S.V., Ruehlemann, C., Chattopadhyaya, U., Pal, J., Chauhan, P.R., Chauhan, 2010. Environmental impact of the 73ka Toba super-eruption in South asia. Reply to the comment on Williams, M.A.J., Ambrose, S.H., van der Kaars, S., Ruehlemann, C., Chattopadhyaya, U., Pal, J., Chauhan, P.R. (Eds.), [Palaeogeography, Palaeoclimatology, Palaeoecology 284 (2009) 295–314]. Palaeogeo. Palaeocli. Palaeoeco. 296 (1–2), 204–211.
Williams, M.A.J., Ambrose, S.H., van der Kaars, S., Ruehlemann, C., Chattopadhyaya, U., Pal, J., Chauhan, P.R., 2009. Environmental impact of the 73ka Toba super-eruption in South asia. Palaeogeogr. Palaeoclimatol. Palaeoecol. 284 (3–4), 295–314.
Wolff, E.W., Chappellaz, J., Blunier, T., Rasmussen, S.O., Svensson, A., 2010. Millennial-scale variability during the last glacial: the ice core record. Quat. Sci. Rev. 29 (21–22), 2828–2838.
Wolff, E.W., 2014. Climate in phase. Nat. Geosci. 7, 397–398.
Xia, Z., Kong, X., Jiang, X., Cheng, H., 2007. Precise dating of east-asian-monsoon D/O events during 95-56 ka BP: based on stalagmite data from shanbao cave at

shennongjia, China. Sci. China Earth Sci. 50 (2), 228–235.
Yuan, D., Cheng, H., Edwards, R.L., Dykoski, C.A., Kelly, M.J., Zhang, M., Qing, J., Lin, Y., Wang, Y., Wu, J., Dorale, J.A., An, Z., Cai, Y., 2004. Timing, duration, and transitions of the last interglacial asian monsoon. Science 304, 575–578.
Zhang, D., Zhang, P., Sang, W., Cheng, H., Wu, X., Yuan, Y., Bai, Y., Wang, J., Jia, J., 2010. Implications of stalagmite density for past climate change: an example from stalagmite growth during the last deglaciation from Wanxiang Cave, western Loess Plateau. Chin. Sci. Bull. 55 (34), 3936–3943.
Zhang, H., Griffiths, M.L., Huang, J., Cai, Y., Wang, C., Zhang, F., Cheng, H., Ning, Y., Hu, C., Xie, S., 2016. Antarctic link with East Asian summer monsoon variability during the Heinrich Stadial–Bolling interstadial transition. Earth Planet. Sci. Lett. 453, 243–251.
Zhang, H., Griffiths, M.L., Chiang, J., Kong, W., Wu, S., Atwood, A., Huang, J., Cheng, H., 2018. East Asian hydroclimate modulated by the position of the westerlies during Termination I. Science 362, 580–583.
Zhang, P., Cheng, H., Edwards, R.L., Chen, F., Wang, Y., Yang, X., Liu, J., Tan, M., Wang, X., Liu, J., An, C., Dai, Z., Zhou, J., Zhang, D., Jia, J., Jin, L., Johnson, K.R., 2008. A test of climate, sun, and culture relationships from an 1810-year Chinese cave record. Science 322 (5903), 940–942.
Zhang, T., Li, T., Cheng, H., Edwards, R.L., Shen, C., Spötl, C., Li, H., Han, L., Li, J., Huang, C., Zhao, X., 2017. Stalagmite-inferred centennial variability of the Asian summer monsoon in southwest China between 58 and 79ka BP. Quat. Sci. Rev. 160, 1–12.
Zhao, J.Y., Cheng, H., Yang, Y., Tan, L.C., Spötl, C., Ning, Y.F., Zhang, H.W., Cheng, X., Sun, Z., Li, X.L., Li, H.Y., Liu, W., Edwards, R.L., 2018. Reconstructing the western boundary variability of the Western Pacific Subtropical High over the past 200 years via Chinese cave oxygen isotope records. Clim. Dyn 52, 3741–3757.